Electrophilic radical coupling at the edge of graphene

Bellunato, A.; Schneider, G.F.

Nanoscale

PAPER

View Article Online
View Journal | View Issue

Cite this: *Nanoscale*, 2018, **10**, 12011

Electrophilic radical coupling at the edge of graphene†

Amedeo Bellunato and Grégory F. Schneider *

We report the selective functionalization of an edge of graphene *via* the electrografting of 4-nitrobenzene diazonium tetrafluoroborate. The edge – a single line of carbon atoms – forms during the process of cutting a graphene monolayer with an atomically sharp microtome knife. Embedded in a polymeric matrix, the just cut bare graphene edge efficiently transfers electrons to a ferricyanide probe in solution. By monitoring the electron exchange reactions of the edge upon functionalization, we observe an annihilation of the reduction and oxidation peaks of the ferricyanide probe, characteristic of the formation of a nitroaryl passivation layer on the edge of graphene. For the first time, the chemical state of a single line of carbon atoms is influenced and monitored using an electrochemical cell, therefore bypassing the usual requirements of atomic resolution characterization techniques, which often demand very clean graphene samples and vacuum processing.

Received 26th April 2018,
Accepted 7th June 2018

DOI: 10.1039/c8nr03429j

rsc.li/nanoscale

Introduction

The selective functionalization of the edge of graphene aims to target the chemically active carbon atoms on the edge without interfering with the sp^2 honeycomb structure of the surface of graphene.[1,2] The abrupt interruption of the conjugated structure of graphene entails the edges with a higher chemical reactivity with respect to the basal plane,[3–11] a consequence of the rupture in symmetry of the lattice. The exclusive functionalization of the edges, however, has hardly been achieved, often relying on bulk methods such as ball-milling and plasma or by polymerizing edge functionalized polycyclic aromatic hydrocarbon monomers.[7,12,13] Here, we selectively functionalize the edge of a graphene monolayer by grafting electrophilic nitrobenzene-aryl radicals in acidic conditions.

The graphene edge is prepared by transverse sectioning of a polymeric block with an embedded graphene film[14,15] using a microtome[16] and an ultra-sharp diamond knife. The mechanical cut proceeds by breaking the lattice of graphene forming an edge. Experimentally, microtomy of graphene from highly oriented pyrolytic graphite (HOPG) yields edges in graphene composed of zig-zag and armchair segments alternated by reconstructed edges where the carbon atoms locally arrange into heptagons and pentagons.[17] Additionally, the cut is performed at the meniscus between water and air, leading to the passivation of the edges predominantly by hydrogenation and hydroxylation.[18,19]

Prior to sectioning, chemical vapour deposition (CVD) graphene is transferred on top of an ultra-flat polymeric substrate containing a metallic gold contact and moulded as a replica of a polished Si/SiO_2 wafer (Fig. 1a-i and ii). The flatness of the substrate preserves the electronic structure of the graphene layer, thereof preventing strains, curvatures or distortions.[20–23]

Next, the graphene layer covered with a film of poly(methyl methacrylate) (*i.e.*, PMMA) is transferred on top of the polymeric substrate and electrically wired (Fig. 1a-iii). Lastly, the PMMA/graphene/polymer stack is further re-embedded inside the polymer block (Fig. 1a-iv). Upon cutting (Fig. 1b), a single line of carbon atoms forms on the surface of the polymer and is constituted by the edge of graphene. Notably, the orthogonal orientation of the graphene with respect to the blade prevents the polymer to fall over and hinder the surface of the edge (Fig. 1c), which is used as an active electrode for monitoring and characterizing electrochemically the edge electrode upon functionalization. In fact, the variation of the electrochemical activity of a graphene edge electrode is proposed as an indirect characterization tool related to the chemical state of a single line of carbon atoms, without employing atomic resolution probe microscopy.[24–27] Specifically, the formation of a passivation layer composed of nitroaryl moieties decouples the edge electrode from the electrochemical probe, indicating the functionalization of the edge of graphene. The binding of a layer of aryl moieties is further characterized by Raman spectroscopy. In fact, the functionalization of the edges of graphene, and the nature of the functionalization (either covalent

Leiden Institute of Chemistry, Leiden University, Einsteinweg 55, 2333CC Leiden, The Netherlands. E-mail: g.f.schneider@chem.leidenuniv.nl

†Electronic supplementary information (ESI) available. See DOI: 10.1039/c8nr03429j

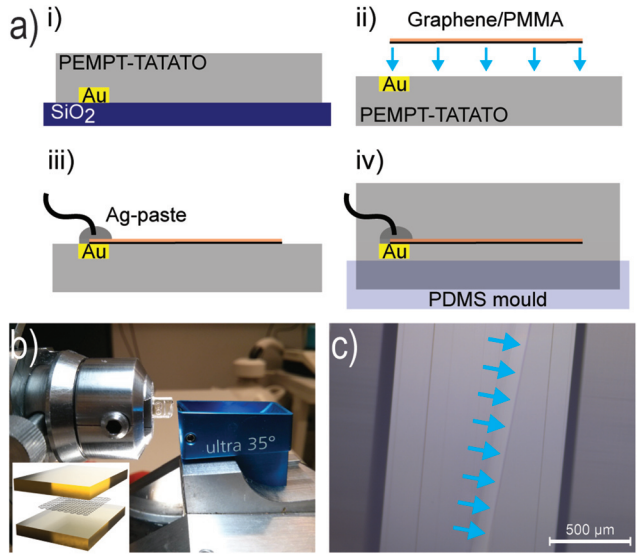

Fig. 1 The graphene-edge electrode. (a) (i) to (iv) embedding of a graphene monolayer within a polymer matrix. (b) Transverse sectioning of the polymer/graphene/polymer block using microtomy. The inset illustrates the embodiment of the graphene inside the polymer. (c) Optical micrograph of the trimmed surface of the polymer–graphene composite showing the graphene edge electrode obtained after the microtomy process. The blue arrows indicate the interface between the polymer and the PMMA coated graphene.

bonding or physisorption) can be addressed by studying the variation of the Raman signature of graphene.[28]

Results and discussion

The graphene edge electrode

Conventional characterization tools such as scanning tunnelling microscopy and atomic force microscopy (STM/AFM) or even highly sensitive elemental analysis like X-ray photoelectron sprectroscopy, can hardly resolve the edge of graphene from the surrounding polymer, specifically because of the organic, insulating nature of the embedding material. The major advantage of graphene is that it is the solely conductive component of the composite sample, thus, as long as the line of carbon atoms is exposed through the trimmed surface of the block, it can be probed electrically and exposed to solvents.

While electrical measurements would require the precise deposition of metal contacts, such as chromium, on top of the trimmed polymer/graphene/polymer edge,[29] we could here monitor the functionalization of the edge by electrochemistry. In fact, the edge of graphene is here the active electrode of an electrochemical cell. The addition of a redox probe such as ferricyanide $K_3Fe(CN)_6$ provides information on the starting electrochemical status of the edge by means of electron exchange reactions between the probe and the edge electrode. Consequently, the mass transport of ions inside the electrolytic solution together with the electron exchange reactions between the electrode and $K_3Fe(CN)_6$ are employed in order to interface the atomically thin graphene edge. This requires the edge electrode to be exposed through the surface of the polymer block. In fact, if the insulating polymer would cover the edge of graphene, a zero potential would develop across the edge electrode and the counter electrode, resulting in a zero-current flow through the cell.

Before electrochemically characterizing the edge, we first studied the quality of the graphene used to generate the edge electrode. As shown in the inset of Fig. 2a, the Raman spectrum of graphene shows a negligible D peak (around 1340 cm^{-1}) and the intensity ratio $I(2D)/I(G)$ between the 2D peak at 2700 cm^{-1} and the G peak at 1590 cm^{-1} is above one, characteristic of single layer graphene.

The electrochemical characterization of the graphene was then first carried in an aqueous solution containing 0.1 M KCl (Fig. 2a) and in 0.1 M KCl supplemented with 5 mM ferricyanide $K_3Fe(CN)_6$ (Fig. 2b). In presence of ferricyanide probe, the cyclic voltammetry presents an oxidation and a reduction peak on the edge of graphene with a minimum and a maximum respectively at 0.23 V and 0.3 V, and with a peak separation of 77 mV at 50 mV s^{-1}. These oxidation and reduction peaks were not detected in KCl solutions without $K_3Fe(CN)_6$ (Fig. 2a). The presence of such peaks suggests the chemical state of the edge

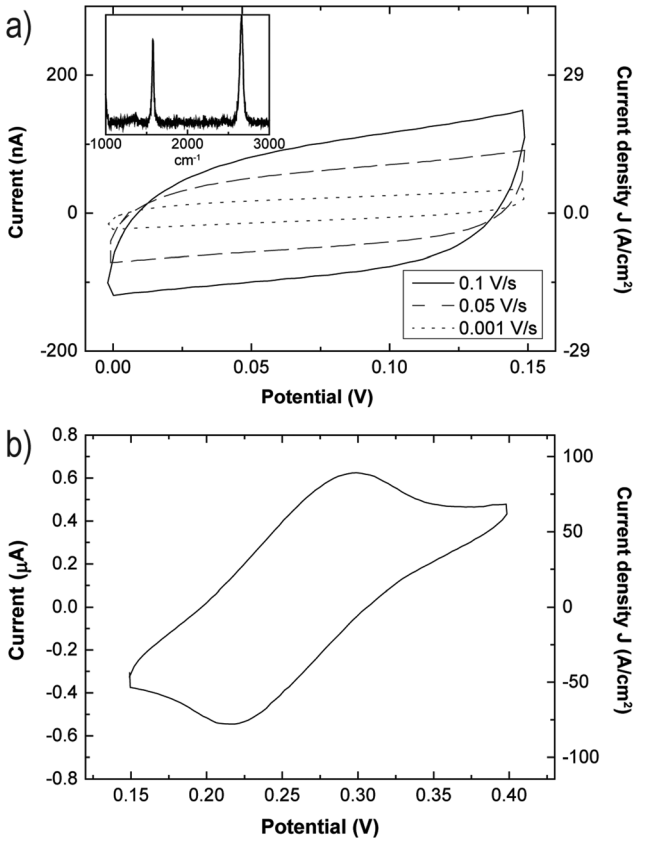

Fig. 2 Characterization of a graphene edge by cyclic voltammetry. (a) Cyclic voltammetry (CV) of a graphene edge electrode in 0.1 M KCl at 0.1 V s^{-1}, 0.05 V s^{-1} and 0.01 V s^{-1}. Inset: Raman signature of a control sample of graphene on Si/SiO_2. (b) CV of the as exposed graphene edge electrode at 0.05 V s^{-1} in 0.1 M KCl and 5 mM $K_3Fe(CN)_6$.

which is deprived of any passivation layer that would otherwise hinder the reversible electron exchange reaction with the probe.

As highlighted by Li *et al.*,[15] at scan rates of 50 mV s^{-1} the cyclic voltammetry curve of a graphene edge electrode assumes a peak shape (Fig. 2b), characteristic of a linear diffusion regime of the electrolytes towards the edge electrode. The associated wave current density, j_p, is described by eqn (1):

$$j_p = \frac{i_p}{S} = 2.69 \times 10^5 n^{3/2} C D^{1/2} v^{1/2} \quad (1)$$

where S is the surface of the electrode, n equals to one and is the number of electrons exchanged in the redox reaction, C is the electrolyte concentration, D the diffusion constant of the electrolyte and v the scan rate. The expected theoretical current density with this model is around 10^{-3} A cm^{-2} at 50 mV s^{-1}, orders of magnitude smaller than our measured peak current density (*i.e.* 85 A cm^{-2}, Fig. 2b). Li,[15] Yuan[14] and Banerjee[30] already noticed such a discrepancy in three different studies concerning graphene edge electrodes, where the current densities varied from 0.11 A cm^{-2} up to 1.2×10^4 A cm^{-2}. Accordingly, Li and Yuan observed a more prominent sigmoidal shape of the cyclic voltammetry curve at lower scan rates. Therefore, they proposed to apply a non-linear diffusion regime,[31] described by eqn (2):

$$j_s = 2\pi FDCL\left[\ln\left(4Dt\left(\frac{\pi}{w}\right)^2\right)\right]^{-1} \quad (2)$$

where F is the Faraday constant, n the number of electrons involved in the redox reaction, C the electrolyte concentration, D the diffusion coefficient,[32] L and w the length and thickness of the graphene electrode, and t defined as $t = RT/Fv$ where v is the scan rate. At scan rates of 50 mV s^{-1} applied to a graphene edge electrode extending over centimeters in length, Yuan also observed a peak shape cyclic voltammetry curve, suggesting the transition to a microscopic linear regime. Our measured steady current of 57 A cm^{-2} (obtained at 50 mV s^{-1}) is therefore in agreement with the theoretical value of 100 A cm^{-2} calculated with eqn (2) and with an edge electrode extending over two millimeters in length. Thus, for a two millimeters long single atom thin electrode at a 50 mV s^{-1} scan rate, we assume a mixed diffusion regime characterized by both convergent and linear diffusion,[33] and thus with higher measured current densities with respect to a purely linear regime.

Consequently, the convergent diffusion could alter the actual diffusion coefficient of the electrolyte, causing such a discrepancy from the theoretical peak current intensity. Other origins could be the quality of the graphene employed in previous studies, such as multilayer graphene[15] and most importantly the preparation of the edge electrode. Particularly, we believe that a rough sectioning and processing of the graphene film have detrimental effects on the quality of the edge.

Electrografting of nitroaryl radicals at the edge of graphene

After the electrochemical characterization of the graphene edge electrode, we electro-grafted aryl radicals from a 1 mM solution of 4-nitrobenzene diazonium tetrafluoroborate (NBD; $BF_4N_2C_6H_4NO_2$) dissolved in an acidic solution of 0.1 M perchloric acid ($HClO_4$). In fact, in acidic environment N_2 is cleaved from the nitrobenzene diazonium, forming an electrophilic nitro-aryl radical[34] with respect to the nucleophilic graphene. The application of a potential difference across the graphene and its counter electrode yields electrophilic reactions, where aryl radicals from NBD bind the edge of graphene (the potential difference increases the energy levels of the electron density of states of graphene overlapping the HOMO's of graphene with the LUMO's of the aryl radicals).[35]

For graphene flakes where both the basal plane and the edges are exposed, the grafting reaction most likely starts at the edge,[36] which are intrinsically more reactive because of the rupture of the sp^2 conjugation. Similarly, grain boundaries and defects have also a higher density of states, therefore competing with the aryl radical grafting reaction. In our work, the selectivity towards the edges of graphene is guaranteed by protecting the graphene basal plane with a polymeric matrix. The reduction of the current density at negative oxidative potentials among the cyclic voltammetry cycles (CV), especially between the first, second and third cycle (Fig. 3a, black curves), is the first proof of the formation of a functional passivation layer on the edge of graphene, with chemical properties similar to

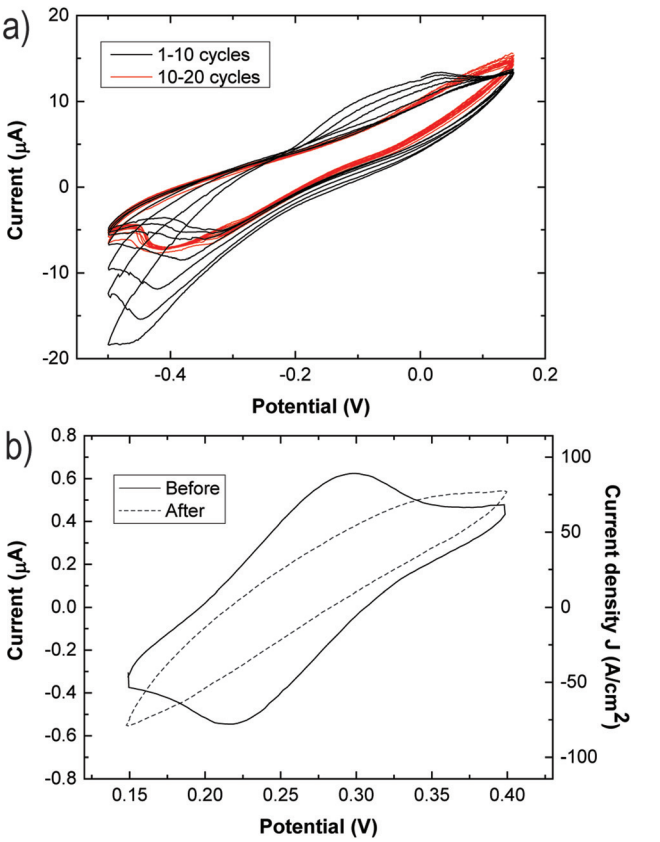

Fig. 3 Functionalization of the edge of graphene. (a) CVs of the graphene edge electrodes in 4-nitrobenzene diazonium in 0.1 M $HClO_4$ at 0.05 V s^{-1}. (b) CVs at 0.05 V s^{-1} CV in 0.1 M KCl and 5 mM $K_3Fe(CN)_6$ before (black curve), and after (dashed curve) the electrografting of the edge.

those reported for the electrografting of nitrobenzene on the surface of graphene.[37] In fact, the NO_2 moieties from NBD constitute an insulating layer passivating the graphene electrode therefore preventing additional binding of nitro-aryl radicals, as confirmed by the stabilization of the CV curves after the first four cycles (Fig. 3a red curves). As a confirmation, Fig. 3b compares the cyclic voltammetry in presence of 5 mM $K_3Fe(CN)_6$ in 0.1 M KCl performed before (black curve) and after (dashed curve) the electrografting of the nitrobenzene aryl-radicals. The formation of an insulating nitrobenzene passivation layer results in the suppression of the electron exchange with the redox-probe in the electrolyte (Fig. 3b, dashed curve), as evidenced by the absence of the redox peaks present before the functionalization (Fig. 3b, black curve).

Characterization of the edge of graphene after functionalization

Subsequently, the functionalization of the edge electrode is investigated by Raman spectroscopy, using a low intensity power laser at 532 nm, shone directly over the polymer/graphene/polymer stack. The red and black crosses in Fig. 4a highlight the location on the sample where the Raman was performed. The inset compares the Raman spectra of the polymer before (red line) and after (blue line) electrografting to exclude the adsorption of nitrobenzene on the polymeric surface. The Raman fingerprints of the polymer arise around 1300 cm^{-1}, 1450 cm^{-1}, 1600 cm^{-1} and 2600 cm^{-1}, without overlapping with the D, G and 2D bands of graphene.

Notably, the Raman signature of graphene (black curve in Fig. 4b) differentiates from the polymer (red curve in Fig. 4b) allowing the characterization of the graphene edge upon diazonium coupling. Particularly, we monitor the variation of the intensity I(D) of the D peak with respect the G peak. In fact, the covalent functionalization of graphene converts the carbons of the honeycomb lattice from sp^2 to sp^3, introducing breaks in the lattice symmetry of graphene and activating the Raman emission mode yielding the D peak. This mode is associated to the stretching of the carbon bonds and requires a defect to be activated.[38] The edges naturally break the periodic lattice of graphene and present an intrinsic D signature,[28,38] as observed by the Raman spectra of graphene in Fig. 4b. The G peak, instead, is an antisymmetric stretching of the carbon bonds within the hexagons of the lattice of graphene.[38] Upon chemical functionalization, the I(D)/I(G) ratio monitors the density and the modification of the sp^3 centers in the lattice of graphene, thus the proceeding of the reaction. At the edges particularly, the formation of bonds influences the vibrations modes activating the D band, modifying its intensity.

Accordingly, upon electrografting (Fig. 4c), we observe the increase of the D peak intensity with respect to the intensity of

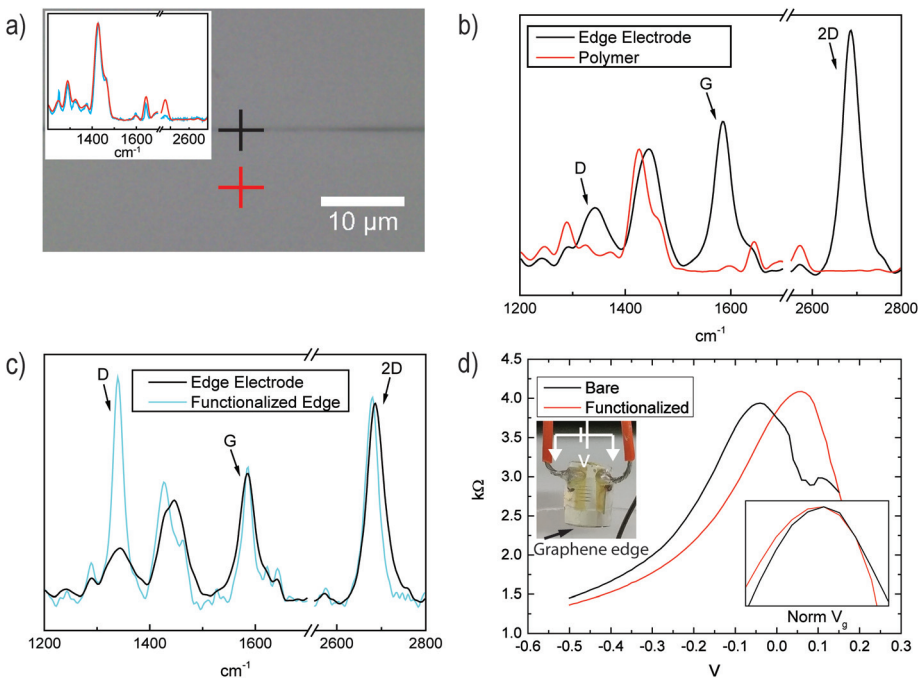

Fig. 4 Raman spectroscopy of the edge of graphene. (a) Optical micrograph of the edge electrode prepared *via* microtomy. Inset: Comparison between the embedding polymer before (red) and after (blue) functionalization of the edge electrode and normalized over the peak around 1450 cm^{-1}. (b) Comparison of the Raman signature of the graphene edge and of the polymer embedding only at the positions indicated by the black and red crosses in panel (a). (c) Comparison between the Raman spectra of the edge of graphene before, and after electrografting of nitrobenzene. (d) Gate dependent conductivity curves of bare (black curve) and functionalized graphene edge (red curve). Left inset: A graphene field-effect transistor embedded in the polymeric matrix and sectioned *via* microtomy. The white arrows indicate the drain and the source. The black arrow indicates the exposed graphene edge electrode. Right inset: Conductivity curves around the Dirac point and normalized at the gate potential of the charge neutrality point.

the G peak, consequently to the covalent functionalization of the edge.[39,40] The Raman results are in agreement with the cyclic voltammetry study: in presence of nitrobenzene diazonium, the edge electrode shows an initial non reversible wave at negative potential (Fig. 3a), which is attenuated in the following cycles. The negative wave rises from the reduction of diazonium moieties into radicals that attack the electrode forming a barrier, physically hindering the electron exchange reaction from the edge electrode to the redox probe.[35,41]

Cyclic voltammetry in Fig. 2a and b, and the Raman spectroscopy in Fig 4c, therefore show the formation of a uniform passivation layer on the edge of graphene. In order to quantify the amount of atoms involved in the reaction, we can model a minimum amount of nitrobenzene grafted to the edge electrode. Referring to density functional theory DFT calculations for the spontaneous grafting of aryl radicals on the edge of graphene, we can estimate that both zig-zag and armchair edges bind 50% of the carbon atoms composing the edge.[42] In a 2 mm long edge electrode there are around $\sim 300 \times 10^{-15}$ mol of carbon atoms, therefore resulting in the functionalization of 150×10^{-15} mol of carbon atoms at the edge.

At last, a graphene field effect transistor (GFET) was used to investigate the selectivity of the electrografting at the edges. For that, a graphene transistor is embedded within the polymer matrix, which edge is exposed *via* microtomy. The transistor (left inset in Fig. 4d) is composed of a drain and a source embedded in the polymer (white arrows). The gate potential is applied to edge electrode *via* an electrolytic solution of 1 M KCl in ultra pure water.[43] By comparing the transistor characteristics of the graphene before and after the functionalization (respectively black line and red line in Fig. 4d), shows that the conductivity of graphene is not affected by the electrografting. In fact, the two curves show the same conductivity values around the charge neutrality point, as well as far apart from the Dirac point. Particularly, the basal plane is chemically preserved during electrografting and only the edge is functionalized (the right inset in Fig. 3d shows the normalized conductivity curves at the charge neutrality points, normalized also with respect to the gate voltage). These results indicate the preservation of the basal plane of graphene during electrografting and the selective functionalization of the edge. In fact, in the case of surface functionalization, the conversion from sp^2 to sp^3 of the carbon atoms composing the honeycomb lattice of graphene would affect its electrical properties, lowering its conductivity and modifying the shape of the resistivity curve close to the neutrality point.[44,45]

Conclusions

To conclude, the present paper reports the selective functionalization of a graphene edge prepared by precise transverse microtomy of a PMMA coated graphene layer embedded inside a polymer matrix. Interestingly, the fine sectioning appears to offer important advantages in the preparation of the edge electrode, firstly re-conciliating theoretical models and experimental results for the convergent diffusion of electrolytes towards sub-nanometric electrodes.

The functionalization step is confirmed through the measurement of the passivation abilities of the nitro-functionalities ahead of the graphene edge against a ferricyanide probe. In fact, the formation of an electrically passivating layer, specifically the assembly of NO_2 functionalities, prevents the reduction of the ferricyanide ions at the graphene edge electrode. The cyclic voltammetry after functionalization is dominated by mass transport rather than redox processes.

The grafting of nitrobenzene at the edge of graphene was also characterized by Raman spectroscopy: the rise in intensity of the D band of the graphene edge confirms the covalent coupling of the nitroaryl radicals selectively on the edge electrode. Conductivity measurements, also, indicate the selective functionalization of the edges, while preserving the integrity of the basal plane. Furthermore, the possibility of a physisorbed layer can be neglected given the established high reactivity of nitrobenzene radicals in acidic conditions.[46]

Importantly, the choice of a NO_2 terminated functional group has the double advantage of being easily detected by means of a redox probe and can be used as a chemical precursor for further functionalization of the edges of graphene.

One of the most important challenge in the chemistry of graphene is to only functionalize the carbon atoms on the edges, for example in edge-based sensors such as nanopores or nanogaps[47] or in nanoribbons graphene field-effect transistors.[48] Thus, the controlled edge chemistry together with methods of characterization of the edge state will open new perspectives to tune the properties of graphene devices in applications ranging from molecular sensing to consumable electronics.

Experimental section

Preparation of the embedding polymer

Pentaerythritoltetrakis mercaptopropionate (PEMPT; *i.e.*, component A), and triallyl triazinetrione (TATATO; *i.e.*, component B) are purchased from Sigma-Aldrich® and mixed in molar proportion 3 : 4 respectively, with 1 wt% of dimethoxy-phenylacetophenone used as photo-initiator. The mixture is degassed under vacuum for about one hour. The polymer is hardened in air under irradiation of a 365 nm UV lamp for 30 min.

Preparation of the graphene layer

Graphene was purchased from Graphenea®, grown *via* chemical vapor deposition on top of a Cu substrate. The graphene is spin-coated with PMMA (PMMA 600K, All Resist GmbH) and back-etched by oxygen plasma at 0.3 mbar O_2, 60 W for 45 s (Diener electronic automated plasma system), in order to remove any trace of carbon from the uncoated side of the Cu substrate. Afterwards the Cu is etched in a 0.5 M aqueous solution of $(NH_4)_2S_2O_8$. Following the etching of the copper, the PMMA coated graphene is rinsed three times with ultrapure water, in

order to remove any trace of etchant from the surface of the graphene.

Transfer of the graphene layer

A drop of polymer is casted and cured onto a Si/SiO_2 wafer patterned with a thermally evaporated gold electrode (around 5×5 mm^2). The polymer contains thiol functionalities, promoting strong adhesion to the gold: the electrode lifts from the oxide surface by intercalating a razor-blade in between the polymer and the surface of the wafer. The lift-off process yields an ultra-flat polymeric substrate embedding a gold contact pad suitable for the electrical connection of the graphene sample. The cured polymer embedding the Au electrode is exposed to an oxygen plasma (0.3 mbar O_2, 60 W for 30 s) in order to convert its surface hydrophilic. The polymeric substrate is dip into a petri-dish containing ultrapure water with the Au electrode facing the water surface. Subsequently, the PMMA coated graphene is transferred on the polymer containing the gold electrode. The transfer proceeds *via* the suction of the water and the gentle deposition of the graphene over the surface of the polymer across the Au electrode. The alignment of the PMMA coated graphene with the gold electrode is performed using a needle and a micro-manipulator.

Microtomy

The polymeric matrix embedding the edge of graphene is first sectioned with a razor blade and then trimmed *via* microtomy, employing a Leica® EM UC 6. Specifically, the sectioned surface is trimmed mounting a Diatome® trimtool 20®, followed by microtomy mounting an Ultra Diamond Knife 35®. The microtomy yields an ultra-flat polymeric surface exposing the edge of a PMMA-coated graphene film, namely the edge electrode.

Cyclic voltammetry

The graphene edge acts as working electrode in a two electrodes system against a Ag/AgCl reference/counter electrode. Cyclic voltammetry characterizations have been performed using an Autolab® potentiostat. The characterization of the edge was performed initially in 0.1 M KCl at 0.1 V s^{-1}, 0.05 V s^{-1} and 0.01 V s^{-1}. The cyclic voltammetry in presence of a redox probe were performed at 0.05 V s^{-1} with a 5 mM solution of $K_3Fe(CN)_6$ in 0.1 M KCl. The functionalization with diazonium salt, $BF_4N_2C_6H_4NO_2$, was carried in a solution of 1 mM $BF_4N_2C_6H_4NO_2$ in 0.1 M $HClO_4$ in Milli-Q water. All the chemicals were purchased from Sigma-Aldrich®.

Raman characterization

Graphene is characterized by Raman spectroscopy on top of a Si/SiO_2 wafer[49,50] (inset Fig. 2a). A sample of PMMA coated graphene is transferred over a Si/SiO_2 substrate. Next, the PMMA is removed with acetone and the sample is rinsed in isopropanol an ethanol. Afterwards, the Raman spectrum is acquired with a 532 nm laser source using a WITec Raman Alpha 3000®.

Electrical characterization

The gating experiments are performed using a lock-in amplifier from Stanford Research System (SR830). The electrical characterization of the graphene transistor is performed in a liquid gating configuration. We use the edge of graphene exposed to a 1 M KCl solution and an Ag/AgCl electrode as the gating electrode connected to the direct coupling, DC, source of the amplifier.

The output voltage of the lock-in is set at 1 V and 77.77 Hz and connected to a 1 MΩ resistor used to impose a 1 μA current through the source of the transistor, while the drain is grounded.

Conflicts of interest

There are no conflicts to declare.

Acknowledgements

We would like to acknowledge the European Research Council under the European Union's Seventh Framework Program (FP/2007–2013)/ERC Grant Agreement no. 335879 project acronym 'Biographene'. We also would like to acknowledge Prof. Dr Bram Koster and Eric Bos of the Leiden University Medical Centrum for providing assistance in the use of the ultramicrotome and Dr. Dennis Hetterscheid and Koen van der Ham for technical assistance on the use of the potentiostat.

References

1 C. O. Girit, J. C. Meyer, R. Erni, M. D. Rossell, C. Kisielowski, L. Yang, C.-H. Park, M. F. Crommie, M. L. Cohen, S. G. Louie and A. Zettl, *Science*, 2009, **323**, 1705–1708.
2 A. Bellunato, H. Arjmandi Tash, Y. Cesa and G. F. Schneider, *ChemPhysChem*, 2016, **17**, 785–801.
3 X. Wang and H. Dai, *Nat. Chem.*, 2010, **2**, 661–665.
4 F. Cervantes-Sodi, G. Csányi, S. Piscanec and A. C. Ferrari, *Phys. Rev. B: Condens. Matter Mater. Phys.*, 2008, **77**, 165427.
5 G. J. Soldano, M. F. Juarez, B. W. T. Teo and E. Santos, *Carbon*, 2014, **78**, 181–189.
6 G. Diankov, M. Neumann and D. Goldhaber-Gordon, *ACS Nano*, 2013, **7**, 1324–1332.
7 T. Kato, L. Jiao, X. Wang, H. Wang, X. Li, L. Zhang, R. Hatakeyama and H. Dai, *Small*, 2011, **7**, 574–577.
8 M. Mooste, E. Kibena, J. Kozlova, M. Marandi, L. Matisen, A. Niilisk, V. Sammelselg and K. Tammeveski, *Electrochim. Acta*, 2015, **161**, 195–204.
9 P. M. Kirkman, A. G. Güell, A. S. Cuharuc and P. R. Unwin, *J. Am. Chem. Soc.*, 2014, **136**, 36–39.
10 D. E. Jiang, B. G. Sumpter and S. Dai, *J. Phys. Chem. B*, 2006, **110**, 23628–23632.

11 J. Greenwood, T. H. Phan, Y. Fujita, Z. Li, O. Ivasenko, W. Vanderlinden, H. Van Gorp, W. Frederickx, G. Lu, K. Tahara, Y. Tobe, H. Uji-I, S. F. L. Mertens and S. De Feyter, *ACS Nano*, 2015, **9**, 5520–5535.
12 Y.-J. Hung, M. Hofmann, Y.-C. Cheng, C.-W. Huang, K.-W. Chang and J.-Y. Lee, *RSC Adv.*, 2016, **6**, 12398–12401.
13 I.-Y. Jeon, Y.-R. Shin, G.-J. Sohn, H.-J. Choi, S.-Y. Bae, J. Mahmood, S.-M. Jung, J.-M. Seo, M.-J. Kim, D. Wook Chang, L. Dai and J.-B. Baek, *Proc. Natl. Acad. Sci. U. S. A.*, 2012, **109**, 5588–5593.
14 W. Yuan, Y. Zhou, Y. Li, C. Li, H. Peng, J. Zhang, Z. Liu, L. Dai and G. Shi, *Sci. Rep.*, 2013, **3**, 2248.
15 K. Li, J. Jiang, Z. Dong, H. Luo and L. Qu, *Chem. Commun.*, 2015, **51**, 8765–8768.
16 Q. Xu, R. M. Rioux, M. D. Dickey and G. M. Whitesides, *Acc. Chem. Res.*, 2008, **41**, 1566–1577.
17 N. Mohanty, D. Moore, Z. Xu, T. S. Sreeprasad, A. Nagaraja, A. A. Rodriguez and V. Berry, *Nat. Commun.*, 2012, **3**, 844.
18 L. Jiang, J. Wang, P. Liu, W. Song and B. He, *RSC Adv.*, 2018, **8**, 11216–11221.
19 A. P. Seitsonen, a. M. Saitta, T. Wassmann, M. Lazzeri and F. Mauri, *Phys. Rev. B: Condens. Matter Mater. Phys.*, 2010, **82**, 115425.
20 a. H. Castro Neto, N. M. R. Peres, K. S. Novoselov and a. K. Geim, *Rev. Mod. Phys.*, 2009, **81**, 109–162.
21 Q. Wu, Y. Wu, Y. Hao, J. Geng, M. Charlton, S. Chen, Y. Ren, H. Ji, H. Li, D. W. Boukhvalov, R. D. Piner, C. W. Bielawski and R. S. Ruoff, *Chem. Commun.*, 2013, **49**, 677–679.
22 V. M. Pereira and A. H. Castro Neto, *Phys. Rev. Lett.*, 2009, **103**, 046801.
23 M. Aslani, C. M. Garner, S. Kumar, D. Nordlund, P. Pianetta and Y. Nishi, *Appl. Phys. Lett.*, 2015, **107**, 183507.
24 Y.-C. Lin, C.-C. Lu, C.-H. Yeh, C. Jin, K. Suenaga and P.-W. Chiu, *Nano Lett.*, 2012, **12**, 414–419.
25 J. Liu, B.-W. Li, Y. Tan, A. Giannakopoulos, C. Sanchez-Sanchez, D. Beljonne, P. Ruffieux, R. Fasel, X. Feng and K. Müllen, *J. Am. Chem. Soc.*, 2015, **137**, 6097–6103.
26 J. Cai, P. Ruffieux, R. Jaafar, M. Bieri, T. Braun, S. Blankenburg, R. Fasel, M. Muoth, A. P. Seitsonen, M. Saleh, X. Feng, K. Mu and K. Müllen, *Nature*, 2010, **466**, 470–473.
27 H. Huang, D. Wei, J. Sun, S. L. Wong, Y. P. Feng, a. H. C. Neto and A. T. S. Wee, *Sci. Rep.*, 2012, **2**, 983.
28 C. Casiraghi, A. Hartschuh, H. Qian, S. Piscanec, C. Georgi, A. Fasoli, K. S. Novoselov, D. M. Basko and A. C. Ferrari, *Nano Lett.*, 2009, **9**, 1433–1441.
29 L. Wang, I. Meric, P. Y. Huang, Q. Gao, Y. Gao, H. Tran, T. Taniguchi, K. Watanabe, L. M. Campos, D. a. Muller, J. Guo, P. Kim, J. Hone, K. L. Shepard and C. R. Dean, *Science*, 2013, **342**, 614–617.
30 S. Banerjee, Â. J. Shim, Â. J. Rivera, X. Jin, D. Estrada, V. Solovyeva, J. Shim, J. Rivera, X. You, J. Pak, E. Pop, N. Aluru and R. Bashir, *ACS Nano*, 2013, **7**, 834–843.
31 D. A. C. Brownson, D. K. Kampouris and C. E. Banks, *Chem. Soc. Rev.*, 2012, **41**, 6944–6976.
32 S. J. Konopka and B. McDuffie, *Anal. Chem.*, 1970, **42**, 1741–1746.
33 C. E. Banks, T. J. Davies, G. G. Wildgoose and R. G. Compton, *Chem. Commun.*, 2005, 829–841.
34 F. Le Floch, J.-P. Simonato and G. Bidan, *Electrochim. Acta*, 2009, **54**, 3078–3085.
35 G. L. C. Paulus, Q. H. Wang and M. S. Strano, *Acc. Chem. Res.*, 2013, **46**, 160–170.
36 H. Lim, J. S. Lee, H.-J. Shin, H. S. Shin and H. C. Choi, *Langmuir*, 2010, **26**, 12278–12284.
37 J. Greenwood, T. H. Phan, Y. Fujita, Z. Li, O. Ivasenko, W. Vanderlinden, H. Van Gorp, W. Frederickx, G. Lu, K. Tahara, Y. Tobe, H. Uji-I, S. F. L. Mertens and S. De Feyter, *ACS Nano*, 2015, **9**, 5520–5535.
38 A. C. Ferrari and D. M. Basko, *Nat. Nanotechnol.*, 2013, **8**, 235–246.
39 R. Sharma, J. H. Baik, C. J. Perera and M. S. Strano, *Nano Lett.*, 2010, **10**, 398–405.
40 Q. H. Wang, Z. Jin, K. K. Kim, A. J. Hilmer, G. L. C. Paulus, C.-J. Shih, M.-H. Ham, J. D. Sanchez-Yamagishi, K. Watanabe, T. Taniguchi, J. Kong, P. Jarillo-Herrero and M. S. Strano, *Nat. Chem.*, 2012, **4**, 724–732.
41 F. Le Floch, J.-P. Simonato and G. Bidan, *Electrochim. Acta*, 2009, **54**, 3078–3085.
42 D.-e. Jiang, A. Bobby, G. Sumpter and S. Dai, *J. Phys. Chem. B*, 2006, **110**, 23628–23632.
43 R. X. He, P. Lin, Z. K. Liu, H. W. Zhu, X. Z. Zhao, H. L. W. Chan and F. Yan, *Nano Lett.*, 2012, **12**, 1404–1409.
44 A. Sinitskii, A. Dimiev, D. A. Corley, A. A. Fursina, D. V. Kosynkin and J. M. Tour, *ACS Nano*, 2010, **4**, 1949–1954.
45 D. B. Farmer, G. M. Roksana, V. Perebeinos, Y. M. Lin, G. S. Tuievski, J. C. Tsang and P. Avouris, *Nano Lett.*, 2009, **9**, 388–392.
46 D. Bélanger and J. Pinson, *Chem. Soc. Rev.*, 2011, **40**, 3995.
47 H. Arjmandi-Tash, L. A. Belyaeva and G. F. Schneider, *Chem. Soc. Rev.*, 2015, **45**, 476–493.
48 W. Fu, L. Jiang, E. P. van Geest, L. M. C. Lima and G. F. Schneider, *Adv. Mater.*, 2017, **29**, 1603610.
49 H. Lu, J. A. Carioscia, J. W. Stansbury and C. N. Bowman, *Dent. Mater.*, 2005, **21**, 1129–1136.
50 R. L. Mays, P. Pourhossein, D. Savithri, J. Genzer, R. C. Chiechi and M. D. Dickey, *J. Mater. Chem. C*, 2013, **1**, 121–130.